THIS PAPER IS A PRE-PRINT OF 10.1109/ITE.2020.2998522 ACCEPTED BY IEEE TRANS. ON TRANSPORTATION ELECTRIFICATION ON 18TH OF MAY 2020 AND AS SUCH IS SUBJECT TO IEEE COPYRIGHT.

Voltage Based Current Compensation Converter Control for Power Electronic Interfaced Distribution Networks in Future Aircraft

Steven Nolan, Catherine E. Jones, Rafael Pena Alzola, Patrick J. Norman, Graeme Burt, Paul Miller, and Mark Husband

***Abstract*—Superconductors have a potential application in future turbo-electric distributed propulsion (TeDP) aircraft and present sig-nificant new challenges for protection system design. Electrical faults and cooling system failures can lead to temperature rises within a superconducting distribution network which necessitate a reduction or temporary curtailment of current to loads to prevent thermal runaway occurring within the cables. This scenario is undesirable in TeDP aircraft applications where the loads may be flight-critical propulsion motors. This paper proposes a power management and control method which exploits the fast acting measurement and response capabilities of the power electronic interfaces within the distribution network to maximise current supply to critical loads, reducing the impact of a temperature rise event in the superconducting distribution network. This new algorithm uses the detection of a resistive voltage in combination with a model-based controller that estimates the operating temperature of the affected superconducting cable to adapt the output current limit of the associated power electronic converter. To demonstrate the effectiveness of this method and its impact on wider system stability, the algorithm is applied to a simulated voltage-source converter supplied aircraft DC superconducting distribution network with representative propulsion motor loads.**

***Index Terms*—TeDP, HEA, Superconductor, Protection, Current Compensation**

I. Introduction

DEMAND for air travel has historically doubled every fifteen years and this trend is set to continue well into the 21st century [1]. However, due to environmental pressures resulting from climate change, governing bodies such as NASA and the EU have set ambitious new performance targets for future aircraft [2], [3]. One potential aircraft concept that can help reach these targets is TeDP. TeDP represents a step change in aircraft electrification, and the resulting power requirements. The gas turbine engines in a TeDP aircraft provide electrical power to electrical motors, with no thrust being directly produced by the gas turbine engines. This allows propulsor motors to be placed at the optimum places on the aircraft to reduce drag and take advantage of boundary layer ingestion (BLI) [4] for example. This significantly improves the aerodynamic performance of the aircraft. However, the

S. Nolan, C.E. Jones, R. P. Alzola, P. J. Norman, and G. Burt are with the Department of Electronic and Electrical Engineering, University of Strathclyde, Glasgow, G1 1XQ e-mail: (steven.nolan@Strath.ac.uk).

P. Miller is with Central Technologies - Future Platforms, Rolls-Royce plc, Derby DE24 8BJ, U.K. M. Husband is with Rolls-Royce Electrical, Rolls-Royce plc, Derby DE24 8BJ, U.K.

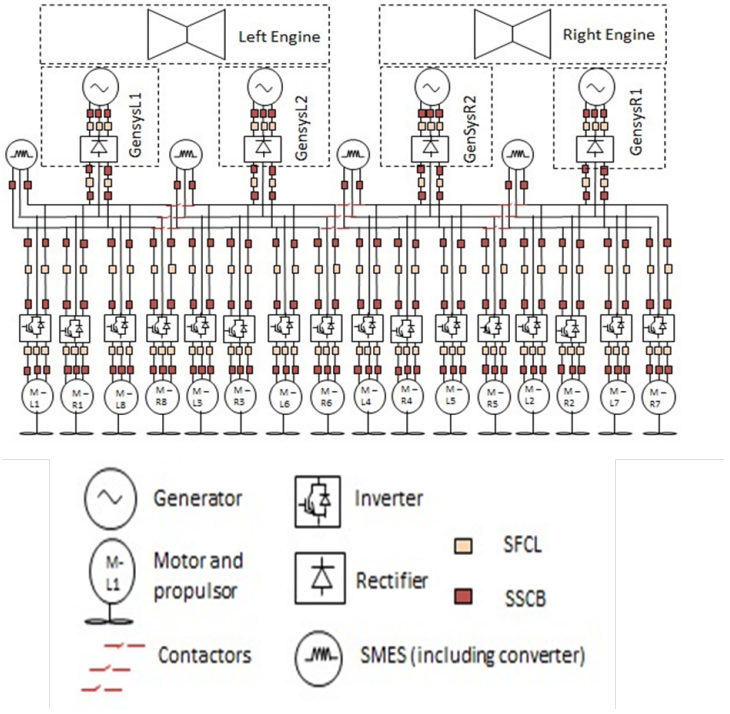

Fig. 1. Example of TeDP architecture that utilises DC distribution [6].

significant increase in the on-board electrical power system capacity required for TeDP (which can exceed 50 MW for large passenger aircraft) must be designed to be as power dense and efficient as possible to realise the full benefits of the TeDP concept [5]. An example DC TeDP network is shown in Figure 1 in which a number of propulsion motors are supplied from a DC distribution network from four generators. The electrical machines are integrated to the DC network using power electronics.

In the near term it is expected that conventional machines will have a high enough power density to achieve a weight-power performance of $7kW/kg$ [7], whilst superconducting machines are expected to offer power densities in excess of $30kW/kg$ [8]. As well, to minimize and manage the thermal load, it is proposed that the distribution system should be superconducting as far as is technologically possible [8]. While the use of superconducting materials offers significant weight reduction and power loss reduction benefits, there are additional challenges due to the cooling requirements of

these systems. This will require progress in cryogenic cooling system density to achieve a performance density of $3kW/kg$ [9]. The additional thermal considerations of superconductors will also entail new protection requirements for the electrical system.

TeDP aircraft include critical loads that require power at all times such as the boundary layer ingestion (BLI) fans which incur a significant drag penalty if de-energised [4]. If a transmission cable undergoes temperature rise, its current capacity will be reduced due to the interdependent nature of the critical parameters: temperature, current, and magnetic field [10]. However, unless the component has exceeded the absolute critical temperature, removing it from service ignores the power capacity still available which can be used to carry current, albeit at a reduced level [11]. This capacity can be used to transmit reduced current to BLI fans to minimise drag penalties and reduce the amount of power that energy storage or backup generators may have to supply in the interim period. This has the potential benefit of reducing energy storage depletion and maximising stability margins in healthy feeders. To implement a control system capable of reduced current transmission, the cable's temperature needs to be estimated from system measurements in a short period of time (for example within milliseconds).

To this end, this paper proposes using fast acting converter control to regulate power flows in distribution lines in which above nominal temperatures are determined, in order to maximise the usage of each asset following abnormal network events. Underpinned by a rapid temperature estimation method, a limiting function is used to reduce current to safe levels and prevent thermal runaway.

This paper is structured as follows: Section II contains a review of the TeDP system requirements and capability for prevention of thermal runaway; Section III introduces the system model for this study, discusses the thermal operating limits of superconductors; Section IV explains the implementation of the converter control method; Section V describes the modelling of the system used for simulation; Section VI contains the results of the simulations while Section VII discusses their impact. Section VIII concludes this paper.

II. TeDP Electrical Power System Requirements

Maintaining the superconducting state requires that a superconducting component operates within the critical surface defined by operating current, temperature and magnetic field strength. Off -nominal conditions, such as electrical faults and cooling system failure can result in the component quenching, transitioning to the conventional state [12]. A consequence of a quench is that due to the resistive nature of a quenched superconducting cable, large amounts of power can be dissipated as heat in the superconductors. If appropriate system management methods are not implemented, this may ultimately lead to thermal runaway and damage to the component [13].

Compared to early superconductors, components made from second and third generation high temperature superconducting (HTS) materials have a larger thermal stability due to an order of magnitude greater heat capacity [14]. This greatly increases thermal stability, enabling the design of fault tolerant components capable of withstanding over- currents without undergoing an excessive temperature rise [15]. Despite this, even a single-figure temperature rise can be enough to reduce critical current substantially, leading to greater losses while also reducing the tolerance of the cable to subsequent electrical faults [16].

Thermal runaway occurs when the cooling system is no longer able to compensate for the losses produced by the component and can lead to the superconducting component suffering irreparable damage [12]. To design superconducting cables to withstand electrical faults, designers can use stability margins which are defined with respect to the current sharing temperature [12]. This temperature is the point at which current begins to transmit through conventional materials built into the cable and is a phase characterised by positive feedback Ohmic losses [12]. The implementation of TeDP, however, requires the use of complex electrical power system architectures with a wide operating range. This is due to power requirements changing in accordance with loading conditions throughout the flight cycle, with take-off and go-around requirements that are around double cruise loading [17]. As discussed in section III, this can cause stability margins to change over the course of the mission which needs to be taken into account in protection system design.

The authors of [13] show how capability curves can be produced for superconducting components. These curves attempt to define the relationship between fault ride -through energy dissipation and the superconducting component's thermal stability [13]. This allows for a relationship to be built between the component experiencing over current and the amount of time that particular current level can be withstood before normal steady state current will lead to thermal runaway. The inability to meet required steady state currents could be an isolation criterion for a conventional, terrestrial system. TeDP however, with arrays of multiple fans that have large operating reserve during cruise can provide for high levels of redundancy and control options [8]. One of these is using converter interfaces to limit and manage current in branches which have undergone temperature rise.

Limiting current in a particular branch through the use of power electronics can be achieved through appropriate converter control [18]. This can give system planners a great deal of design freedom that can be used to help prevent abnormal conditions from affecting flight. The ability to limit current using converters will be dependent on the architecture of the distribution system as well as the capability of the power electronic module. In particular, the load types used in the system could play an important role in ensuring system stability [19]. For instance the influence of constant power and constant impedance loads will be investigated in this paper to determine their influence on network stability and thermal runaway during implementation of a current limitation control method.

In this area there is a significant amount of existing literature on DC micro-grids which is directly applicable to a TeDP system with respect to control and system stability. For instance the authors of [20] examine the impact of parallel

sources on the stability and reliability of a more-electric aircraft (MEA) DC aircraft bus with CP loads, concluding that energy storage is essential to improve these attributes. Coordinating load sharing between multiple sources in a DC-microgrid can be done through droop control [21]. While this type of control has been applied to MEA concepts such as in [20] and [22], the application of load sharing techniques is not well explored with respect to superconducting systems and the additional constraints introduced by the use of these materials. For instance, no literature explores the application of these techniques resulting from a superconducting cable requiring current limitation due to operating at higher than normal temperatures.

As well as load sharing strategies to reduce the current carried by a superconducting cable, power management and load shedding strategies can be adopted to reduce the power consumed by specific loads and reconfigure the network the deliver power through alternative paths as proposed by [23]. Within conventional MEA load management strategies are reviewed by [24] where specific strategies suggested involve exploiting loads with large time constants such as galley ovens, and exploiting the cyclical nature of certain loads such as wing ice protection [25]. However owing to the power levels of electrical propulsion for large commercial transport, such methods may not remove enough demand on the electrical power system to reduce current to safe levels and a combination of network reconfiguration and curtailment of propulsion loads may be required.

To limit current effectively while ensuring appropriate safety margins are kept, the temperature of the superconducting component must be known. Thermal measurements can be used for this however the response time of the measurements can vary significantly depending on the sensor used and the application itself [26]. These response times may be too large to limit current before thermal runaway takes place. An alternative approach is to estimate the temperature of the component through electrical measurements. This paper presents a method that uses the IV-characteristic of the superconducting transition to determine the temperature of the component in real time and adjust current to a suitable level.

III. Development of Maximum Recovery Temperature Model

A. System Model for Analysis

The control method developed in this section is applied to the system shown in Figure 2, which considers a single generator and motor channel taken from the overall TeDP network (Figure 1) with an energy storage source connected to the common bus through a DC/DC converter. This electrical architecture consists of a three-phase generator that is supplying electrical power to the distribution system, which includes a single propulsion motor load. The two electrical machines interface to a DC distribution network via power electronic converters. The distribution network consists of a superconducting cable and a DC filter capacitor that reduces voltage ripple at the output of the active, six-switch rectifier which interfaces the generator to the network. A low impedance

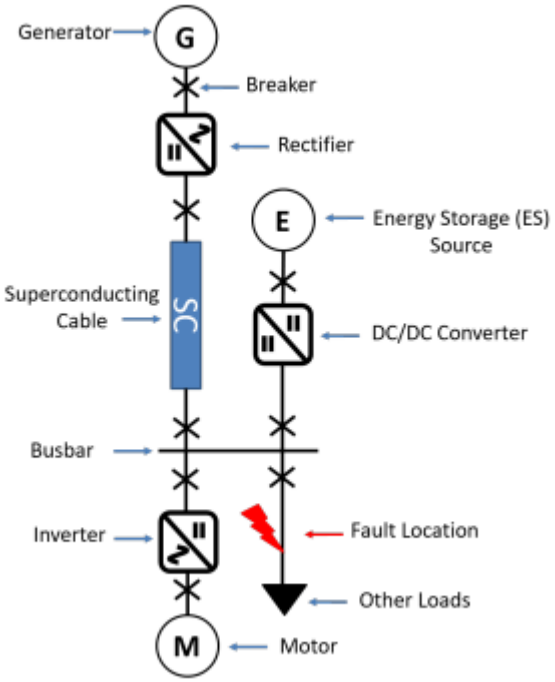

Fig. 2. High level diagram of system for modelling.

fault is located downstream of the superconducting cable as indicated on Figure 2 which will be used to demonstrate a heat generating event that requires cable current limitation to prevent thermal runaway. This architecture does not include an superconducting fault current limiter (SFCL), this is to ensure that the cable's temperature rises during the fault. All modelling was carried out within Mathworks' MATLAB Simulink software package. Key model parameters are provided in Table 1, in Section V.

B. Superconducting DC Distribution Cable

The superconducting DC cable is a thermal-electric cable model that includes a conduction layer made up of Yttrium-barium-copper-oxide (YBCO) superconducting material and a conventional copper shunt. The conduction layer is wound around a layer of insulation separating it from the former. Another layer of insulation separates the conduction layer from the shield. The shield is assumed to be identical in its electrical characteristics to the conduction layer. The design of this cable is illustrated in Figure 3. To calculate current sharing between the superconducting and conventional materials in the component, a current iterative algorithm adapted from [27] is used.

C. Current-Temperature Operating Requirements of a Superconducting Cable

This subsection describes the development of the V4C specific theoretical models that underpin the new control method presented in Section 4. To develop thermal operating limits with respect to required operating current, two terms

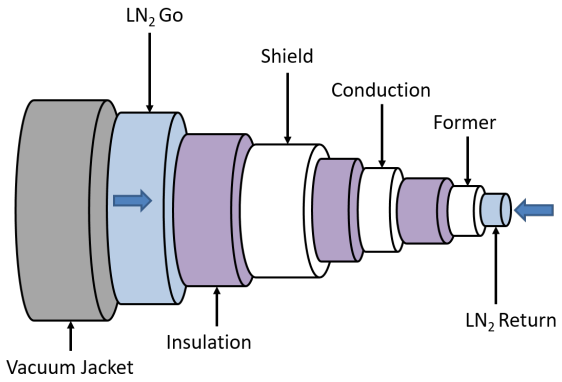

Fig. 3. Illustration of superconducting cable's physical description.

are now defined: maximum recovery temperature (MRT), and maximum recovery current (MRC). These operating limits will be used to calculate safe current limits that the rectifier on Figure 2 will be allowed to output following a temperature rise. MRT is defined as the maximum temperature the component can carry a given load current without thermal runaway occurring due to power losses incurred from operating near the critical current. MRC is the maximum current that the component can operate at a given temperature without electrical losses leading to thermal runaway. Utilisation of these criteria allows for the selection of a safe maximum operating current following a heat-generating event. This will prevent unnecessary curtailment of current during flight phases in which significant spare current capacity exists to meet the required demand.

At the MRT the losses produced by the component, in Joules, Q_{in}, are equivalent to the amount of heat the cooling system can remove, Q_{out}. These values can be calculated for a circular geometry of a cable operated in DC, where the primary loss mechanism considered is due to flux-creep, flux-flow and current sharing with conventional materials [28]. This is caused by operation near and above I_c. The Equations for Q_{in} and Q_{out} are shown in (1) and (2) respectively. Within the thermal modelling of the cable, heat intrusion sources are neglected as they are assumed to be a much smaller source of heat than that produced by flux-flow and Ohmic losses in the cable when operating at or above critical current [28], which are the operating conditions of interest in this paper. Additionally, the temperature of the cryogen used to cool the cable is assumed to be constant.

$$Q_{in}(t) = I_{sc}(t)V_{sc}(t) \tag{1}$$

$$Q_{out}(t) = hA(T(t) - T_{cool}(t)) \tag{2}$$

Where h is the heat transfer coefficient in W/m^2K, A is the surface area of the cable in m^2, and $T_{cool}(t)$ is the temperature of the coolant in Kelvin, T is the temperature of the cable, I_{sc} and V_{sc} are the current carried and voltage dropped across the cable respectively. The temperature of the cable is calculated in accordance with (3), where $C_v(J/m^3)$ represents the volumetric heat capacity of the cable while the initial temperature is given by $T_0(K)$.

$$T(t) = T_0 + \frac{1}{C_v}\int_0^t Q_{in}(t) - Q_{out}(t) \;\; dt \tag{3}$$

Superconducting materials create an electric field, $E(V/m)$, in response to the flow of current. The magnitude of this field varies exponentially in accordance with the power law [10] and the ratio of the instantaneous current magnitude, $I_{sc}(t)$, to the temperature dependent critical current, $I_c(T)$. Assuming uniform superconducting properties in the direction of the transport current, the voltage dropped, $V_{sc}(I,T)$ along a length, $L(m)$, of superconducting material can be calculated using (4). Where α is the transition index, which describes the steepness of the transition between the superconducting and conventional conduction states, and E_c is the quench voltage constant, $100\mu V/m$.

$$V_{sc}(I,T) = E_c L \left(\frac{I_{sc}(t)}{I_c(T)}\right)^{\alpha} \tag{4}$$

The temperature dependent critical current can be calculated according to (5) while the temperature dependence of the transition index is calculated according to (6) where T_c is the critical temperature and T_{ref} is a reference temperature. I_{cref} and α_{cref} are the critical current and transition index measured at a reference temperature while the indices k and β describe the nature of the temperature dependence for the critical current and transition index respectively [29].

$$I_c(T) = I_{cref}\left(\frac{T_c - T}{T_c - T_{ref}}\right)^{k} \tag{5}$$

$$\alpha(T) = \frac{\alpha_{ref} - 1}{2}\left(\frac{T_c - T}{T_c - T_{ref}}\right)^{\beta} + 1 \tag{6}$$

At the MRT (1) and (2) are equal in value. By substituting (4) into (1), (7) is arrived at, where T_{MRT} is the MRT and $Q_out(t, T_{MRT})$ the heat removed at the MRT.

$$I_{sc}(t)E_c\left(\frac{I_{sc}(t)}{I_c(T_{MRT})}\right)^{\alpha} = Q_{out}(t, T_{MRT}) \tag{7}$$

Rearranging (7) allows for the maximum current carried by the cable at the MRT to be calculated, as given in (8). As an example of this relationship, Figure 4 shows the output of (8) for a cable with a critical current of $1000A$ operating with a coolant temperature of $77K$, the boiling point of liquid nitrogen under atmospheric pressure.The heat removed is assumed to be constant along the length of the cable at $0.2W/mK$. The rapid rise between $0A$ at $77K$ and the peak value is because heat does not flow between two bodies of equal temperature.

$$I_{MRC}(t,T) = \sqrt[\alpha+1]{\frac{I_c(T_{MRT})^{\alpha}Q_{out}(t,T)}{E_c}} \tag{8}$$

IV. Voltage-Based Current Compensation Converter Control (V4C)

The proposed method aims to maximise the amount of power that can be transmitted through a converter interfaced

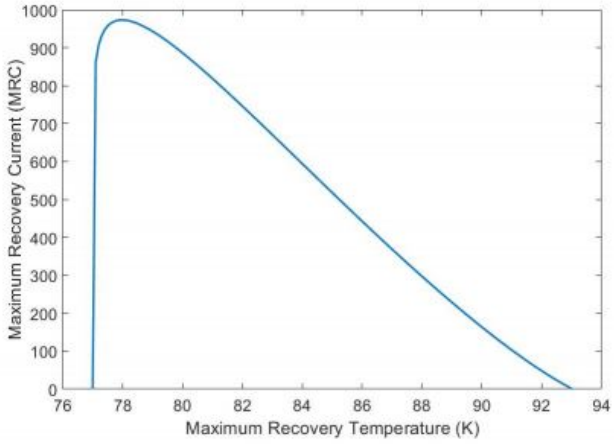

Fig. 4. Example of maximum recovery current (MRC) w.r.t maximum recovery temperature (MRT).

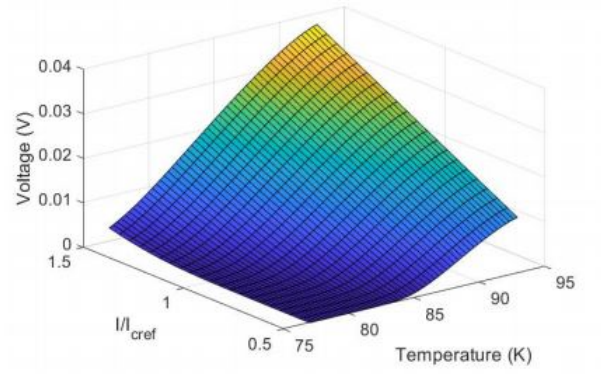

Fig. 5. Surface of voltage drop w.r.t. temperature and current of a superconducting distribution cable. Current is normalized here for readability as it is the ratio of instantaneous current to critical current that determines the voltage drop in a superconducting cable (Equation 4).

distribution line forced to operate at temperatures greater than nominal. To do this, temperature must be estimated to ensure that current is curtailed to a level that prevents losses from leading to thermal runaway of the superconducting feeder cable. This is achieved using knowledge of the components voltage response at different currents and temperatures in order to determine safe operating values for the present conditions.

The voltage response of a superconducting cable to an input current is strongly temperature dependent which can be seen in (4), (5) and (6). By determining the current flow in the superconducting material for a given shunt impedance, it is possible to derive the voltage drop across the cable for a range of input current and temperature magnitudes (using Equation (4)) which can then be visualised in a 3D surface plot (shown in Figure 5, created in this instance using a shunt resistance of $2.5m\Omega$).

Assuming the cooling system is active, the maximum current limit for the superconducting cable can be calculated using (8). An operating current below this boundary can be selected which will then allow temperatures to return to nominal

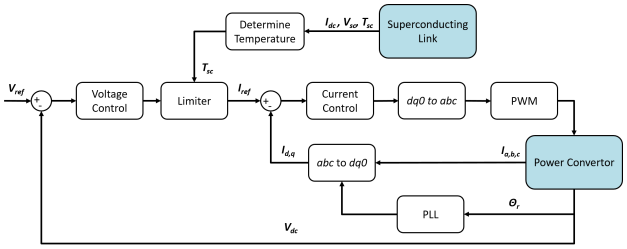

Fig. 6. V4C implemented as feed-forward loop within a dq-controlled rectifier.

operating levels, while providing partial load fulfilment during this period. In practice a look-up table could be used to quickly ascertain this temperature based on the components voltage response at a given current input temperature. This provides a fast and simple procedure for estimating the temperature based on electrical magnitudes which can then be used to to limit current in a converter control scheme as will be shown in the following sections of this paper.

Alternatively, the temperature can be estimated from (9), which is derived from substituting (5) into (4) and rearranging for T. Although a greater margin of error when using this equation is needed as α must be constant to prevent an algebraic loop.

$$T = T_c - \left(\left(\frac{\left(\left(\frac{E_c^{1/\alpha} L^{1/\alpha}}{V_{sc}(t)^{1/\alpha}} \right) I_{sc}(t) \right)^{1/n}}{I_{cref}^{1/n}} \right) (T_c - T_{ref}) \right) \quad (9)$$

This limitation of current is implemented via the use of a feed-forward controller within a power electronic control system. The feed-forward controller is designed to saturate the current request to stay within the safe operating boundary of Figure 4 at all operating temperatures up to T_C, where the component has lost all superconducting properties.

V. Application of Method to a TeDP Electrical Power System

A. Rectifier Control

This section describes the control of the power electronic interfaces of the system shown in Figure 2. The control of the rectifier used to interface the generation source with the network is described in Figure 6. As shown in this Figure, the rectifier uses a direct-quadrature (dq) control scheme designed to regulate the output DC voltage and current to $1pu$. The capacitor is sized in accordance with [30] to be 4.3mF. This approach to the modelling of the system's three-phase generator and rectifier is done in accordance with [31]. However, component non-idealities and parasitics have been ignored as their impact on the system response for the studies in this paper are negligible.

The generator is modelled as a three-phase controlled voltage source with a rated power of 1 MW as shown in table 1. A phase locked loop (PLL) is used to determine the rotor angle, θ, of the generator for use in the $dq0$ transform (10). The transform is applied to the three phase currents of the generator.

$$\begin{bmatrix} u_d \\ u_q \\ u_0 \end{bmatrix} = \frac{2}{3} \begin{bmatrix} \cos(\omega t) & \cos(\omega t - \frac{2\pi}{3}) & \cos(\omega t \frac{2\pi}{3}) \\ -\sin(\omega t) & -\sin(\omega t - \frac{2\pi}{3}) & -\sin(\omega t + \frac{2\pi}{3}) \\ \frac{1}{2} & \frac{1}{2} & \frac{1}{2} \end{bmatrix} \begin{bmatrix} u_a \\ u_b \\ u_c \end{bmatrix} \tag{10}$$

The controllers are designed to control the direct and quadrature currents which individually correspond to the real (direct) and reactive (quadrature) power output of the rectifier. Hence the quadrature component (I_q) is controlled to be zero. The direct current, (I_d), changes with respect to reference requests from the voltage control loop. It is assumed that the three phase system is balanced and that the zero component is a constant at 0. The voltage control loop measures the voltage across the DC filter capacitor and compares it to a set reference that is nominally $1pu$. The error signal is then passed through a PI controller to generate the reference current, I_d^*.

The direct current request is compared to I_d, and passed through a second PI controller. An inverse dqo transform is applied to the controller outputs and passed to the modulator which implements pulse width modulation (PWM) for controlling the rectifier switches. The gain and time constants for the PI controller are set in accordance with [32] and accounts for the delay inherent in discrete sampling.

B. V4C Control Implementation

V4C is implemented, as shown in Figure 6, using feed-forward compensation. As described in Section 4, this method uses the measured resistive voltage drop across the superconducting cable and the current output of the 3 phase rectifier to determine the operating temperature of the cable. Following temperature determination the current request from the voltage control loop is saturated to a value lower than the MRC for this operating temperature using (11). This allows current to be limited quickly, without interfering with the operation of the system during normal conditions.

$$I_{max} = kI_{MRC}(T) \tag{11}$$

Where k is less than or equal to 1 and can be adjusted to provide a suitable current margin for the cable and allow for cooling system to remove energy and reduce temperature. To prevent integral wind-up occurring within the voltage control loop, the saturation limits of the integral component of the PI controller are set to be the maximum normal operating point of the superconducting cable. This ensures that when temperatures return to their normal operating conditions, that the voltage control loop is able to quickly resume control.

C. Back-up Energy Source

The energy storage (ES) depicted in Figure 2, can be any energy storage source such as a battery, superconducting magnetic energy storage (SMES), or a normally open point that feeds power from secondary electrical generators following network reconfiguration. Within the model ES is represented as a controlled current source input with operating current being determined through DC droop control [33]. This allows for effective power sharing between multiple generation sources without the need for communication. The energy source only discharges once the measured network voltage drops below 0.94pu to prevent discharge during normal voltage variations, in accordance with terrestrial standards for voltage limits in the UK. The speed at which the back-up power source can respond to a power request is limited by bandwidth of its controller. This bandwidth is set as an order of magnitude slower than the bandwidth of the 3-phase rectifier using a low-pass filter with a bandwidth of 1 kHz at the control signal input. This ensures the ES will only transfer energy into the system in response to voltage deviations when the superconducting link is unable to meet the demand during abnormally high-temperature conditions. Additionally the maximum power output of the back-up energy source is arbitrarily assumed to be 30% of the full load requirements of the motor.

TABLE I
SIMULATION PARAMETERS

Parameter	Unit(s)	Value
Superconducting Material	Type	YBCO
Transition index (at 77K)	n.a	20
Cable Operating temperature	K	77
Critical Temperature	K	93
Critical Current	A	1200
Rated DC Voltage	V	1000
Cable Length	m	100
Conventional Resistance	Ω	0.0025
Rated AC Voltage	V	615
DC Capacitance	mF	4.3
Constant Impedance Load R	Ω	1
Constant Impedance Load L	mH	1
Cooling coefficient	W/mK	0.2
Rated Power	MW	1

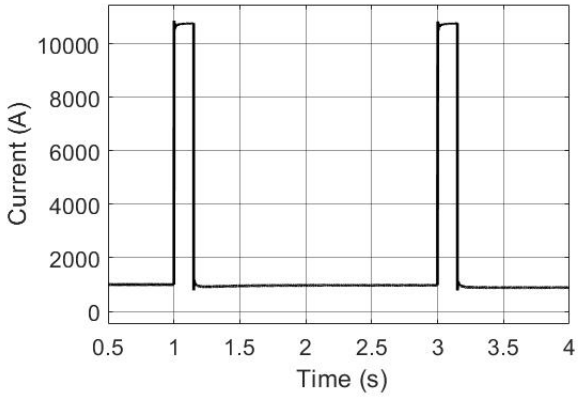

Fig. 7. $10kA$ Fault current implemented on network using controlled-current source downstream of the distribution cable and subsequently cleared after $150ms$. This is implemented twice, once at $1s$ and again at $3s$.

VI. Results

To investigate the effectiveness of the proposed control method, with respect to different load types and system architectures, multiple scenarios are considered. Two network architectures are investigated: a system containing a backup power source, Figure 2, and a network in which the backup energy source is not present. How the presence of additional power supplies can affect the ability to implement the proposed control scheme, and the impact on the stability of the network following current reduction, is discussed.

The types of load considered for these two network architectures are constant power (CP), where the motor's power controller will attempt to maintain a constant power to the load by varying the impedance seen by the network, and constant impedance (CI), in which the motor will draw current in proportion to network voltage conditions. These two load types are chosen due to their differing response to the system voltage conditions. Due to the nature of these load types it is expected that any control algorithm that limits current could have a subsequent impact on system voltage stability. This needs to be investigated to determine the limits of the V4C method in networks with these load types. As well as these scenarios, the implementation of the V4C controller within the motor's inverter control scheme is also investigated. This scenario presents the case in which a power management system is able to implement load shedding to preserve the thermal stability of the superconducting network.

The component values for the Matlab network simulation are shown in Table 1. The superconducting cable is modelled in accordance with Section 3.B for the parameters specified in Table 1. This model is used to populate a lookup table which describes the voltage response of a superconducting cable over wide range of current and temperatures values. This is used to determine the operating temperature throughout the course of the simulation. For these simulations a fault current of $10kA$ DC is used in order to cause significant temperature rise in the superconducting cable. The fault is removed from the system after $150ms$ to simulate the opening of mechanical circuit breakers. The fault current is implemented using a controlled current source within the Simulink software package.

The temperature rise due to the fault causes the critical current of the material to decrease. This leads to a voltage being generated across the superconducting cable and Ohmic losses occurring even after current returns to normal operating levels. In this condition, the feed-forward control loop will estimate the new operating temperature in accordance with Figure 5 and a new safe maximum current is chosen to prevent thermal runaway of the cable. To implement this control action, the current request, I_d^*, created by the voltage controller, is saturated to ensure this maximum current level is not exceeded.

Two faults are applied during the course of the simulation, occurring at 1 and 3 seconds into the simulation as shown on Figure 7. This emulates the situation in which multiple faults occur within the system in succession. The results demonstrate that the V4C controller will not take action during the first fault, because current limitation is not required to preserve thermal stability but will act after a subsequent fault that leads to temperature rise above the MRT, at which point the superconductor can no longer supply the requested current without thermal runaway taking place.

Figures 8a and 8b show the filter capacitor voltage and DC current profiles for scenarios in which a CI load is being fed by the system. These figures show the impact of current limitation taking place at the rectifier for architectures with and without ES. Figures 9a and 9b show the filter capacitor voltage and DC current profile for scenarios in which the CI load has been replaced with a CP load. Figures 10a and 10b show the filter capacitor voltage and DC current profile for the scenario in which V4C control is implemented within the inverter control loop in order to show how the placement of the controller can affect network stability.

Figure 11 shows the temperature of the superconducting cable for each scenario. Figure 11 has been extended over a period of $10s$ to show whether thermal runaway or thermal recovery takes place after each fault scenario is implemented with the V4C controller in use.

VII. Discussion

In the case of CI loads, reducing upstream current output requires a reduction in system voltage unless the network is able to provide power from an alternative source. This is due to the energy imbalance between the power requested by the load and power delivered by the generator. This can be seen in Figures 8a and 8b which show that an alternative power source will be required to ensure network voltage does not drop below required limits while providing a full range of current limitation. Without this alternative source, the maximum current limitation will be determined by the under-voltage limit of the network. Hence, the minimum current the converter can supply, determined by network minimum voltage limits, may not be sufficient to reduce current below MRC. This can be seen on the black dashed line in Figure 11, where the temperature rise continues following current reduction as the rectifier is incapable of reducing current enough to prevent thermal runaway, as shown on Figure 8b. With the ES to support network voltage however, the superconducting feeder is able to supply a portion of the current, Figure 8b, while temperatures stabilize, Figure 11. In this case the maximum amount of current limitation that can be applied is dependent on the maximum amount of power that the ES can supply. In this case the maximum amount of power the ES can supply is set at 30% of full load. If current must be limited to the extent at which the energy source must supply greater than this amount, then network voltage will begin to decrease which can lead to under-voltage protection tripping.

Within a DC TeDP distribution network the motor loads will be interfaced through inverters. If these inverters tightly regulate their loads, they can appear as CP loads which have a negative impedance characteristic. This means that any attempt to reduce current will cause the DC network voltage to decrease, Figure 9a, and consequently cause the inverter to draw more current, Figure 9b, to maintain CP. This causes a further depression of system voltage, potentially leading to

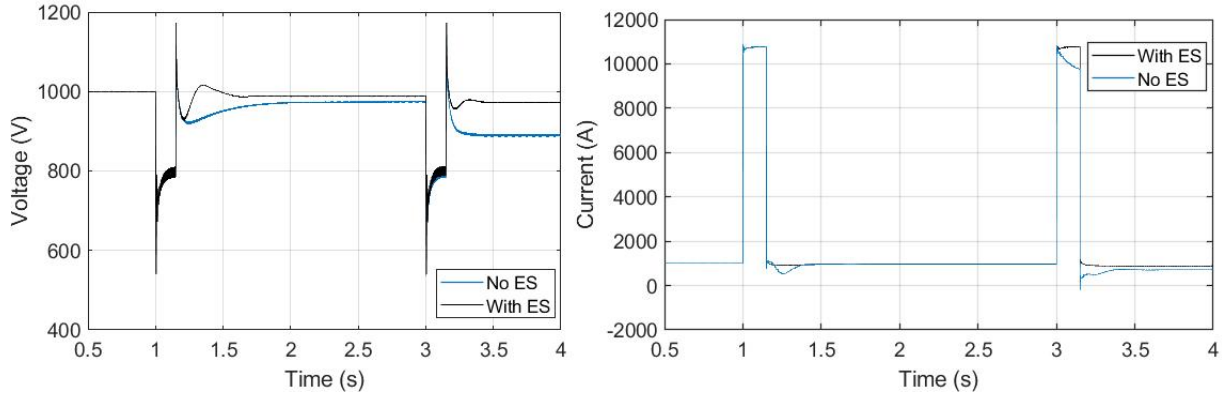

Fig. 8. a) DC voltage for V4C control implemented on a dq-controlled rectifier with a constant impedance load with and without a back-up energy source. b) DC current profile for V4C control implemented on a dq-controlled rectifier with a constant impedance load with and without a back-up energy source.

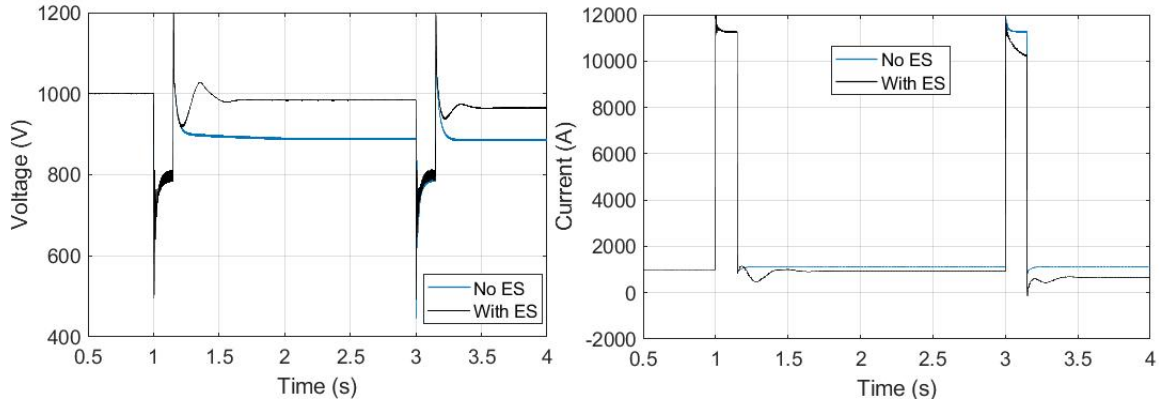

Fig. 9. a) DC voltage for V4C control implemented on a dq-controlled rectifier with a Constant power load with and without a back-up energy source. b) DC current profile for V4C Control implemented on a dq-controlled rectifier with a constant power load with and without a back-up energy source.

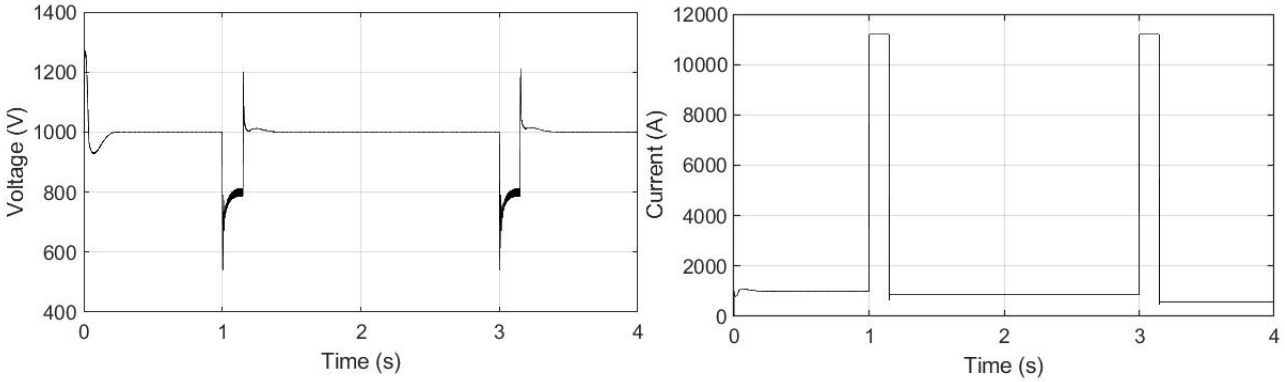

Fig. 10. a) DC voltage for V4C control implemented on a motor inverter. b) DC current profile for V4C control implemented on a motor inverter.

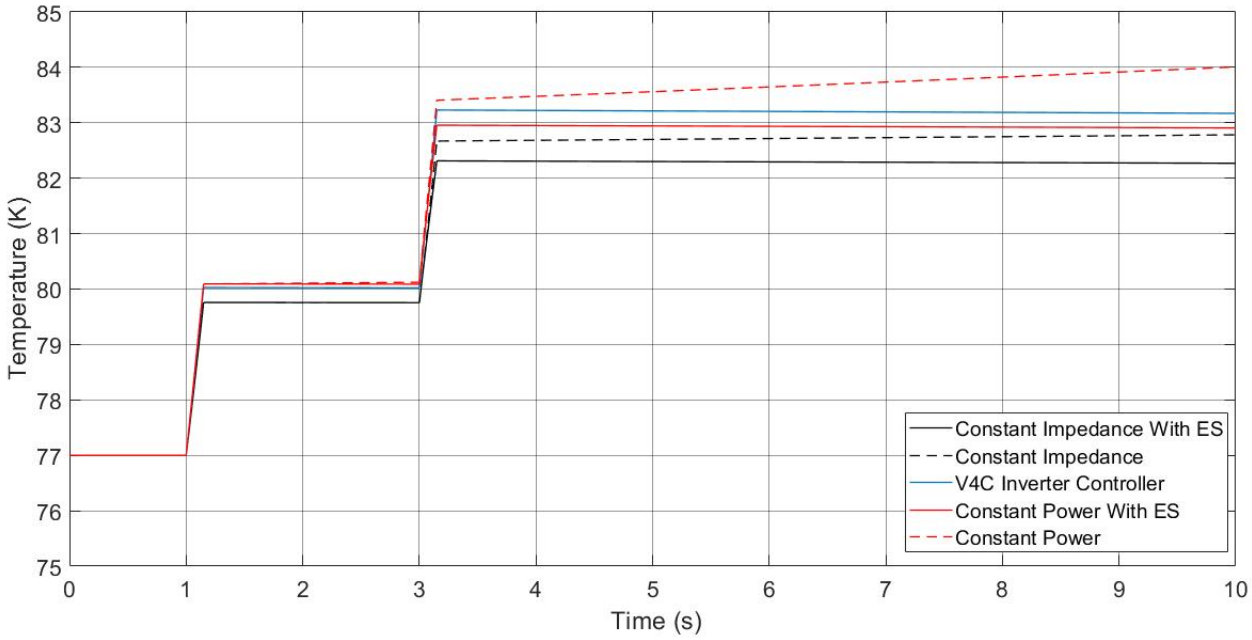

Fig. 11. Comparing temperature recovery of superconducting cable in different system architectures utilizing V4C.

quicker thermal runaway due to the larger current drawn. This can be seen in Figure 11, dashed red line, in which thermal runaway takes place quicker than other scenarios due to the greater current request from CP load, Figure 9b.

This potentially damaging issue can be resolved if the network contains a sufficient energy storage source, downstream of the affected feeder, that is able to provide the power required to prevent significant voltage deviations. This allows the feeder to supply partial power while temperatures return to normal. Alternatively, the network can be reconfigured to provide power from a different generator feeder. This scenario is shown in the blue lines in Figures 10 and 11, where the application of a droop controlled energy storage source is able to ensure that the DC network voltage is maintained. This allows full power to be delivered to the motor while ensuring the network's thermal and voltage stability is maintained.

An alternative solution is the placement of the feed-forward limiting block within the inverter connected to the propulsion motors such that the component reduces its current request when it detects abnormal temperatures either upstream or within the motor, Figure 10b. This allows for the power drawn by the motor to be reduced to ensure voltage stability within the network, Figure 10a, while also preserving the distribution networks thermal stability, Figure 11. While allowing for these benefits, it would require coordination to ensure aircraft dynamics are not negatively affected by reduced thrust output of the motor. This could be exacerbated in architectures, such as the N3-X TeDP network shown in Figure 1, which contain large numbers of motors being fed by a single channel and would require greater coordination to ensure appropriate limitation of current and equal distribution of thrust across multiple fans.

Without the V4C approach adopted in this paper, current is limited based on the maximum that can be transmitted through the conventional materials present in the superconducting cable without exceeding the cooling system's capacity. For instance, based on the parameters shown in Table 1, and assuming that the temperature of the liquid nitrogen reservoir remains constant, the current would have to be limited to approximately $320A$ to prevent the temperature of the cable from exceeding T_C. This is lower than the amount of current capable for being provided by the cable using a V4C control as illustrated in Figure 12 which compares the cable MRC and the maximum current level that can be transmitted through the conventional material (when no superconductivity is present) to maintain a given temperature. The limitation of current transmission through conventional materials can be increased by using larger cross-sectional areas of conventional material in the cable's design, but this will increase weight, which is a key design variable in aircraft systems. This greater current restriction also increases the amount of power that needs to be supplied by additional sources such as ES, further driving up system mass.

VIII. Conclusion

Superconducting components are a potential enabler for future aircraft electrical systems due to their high power densities. To maximise the benefits of superconducting technologies, robust system management is needed to accommodate the unique thermal requirements of these components without negatively impacting flight if an abnormal event occurs, causing the temperature of the superconducting cables to rise.

Results in this paper have shown that in the case of a superconducting cable being subjected to a temperature rise, which prevents conduction of full load current, the proposed method maximises power flow in the cables without thermal runaway occurring. This is of particular benefit for TeDP aircraft where it is highly desirable to maintain power to BLI

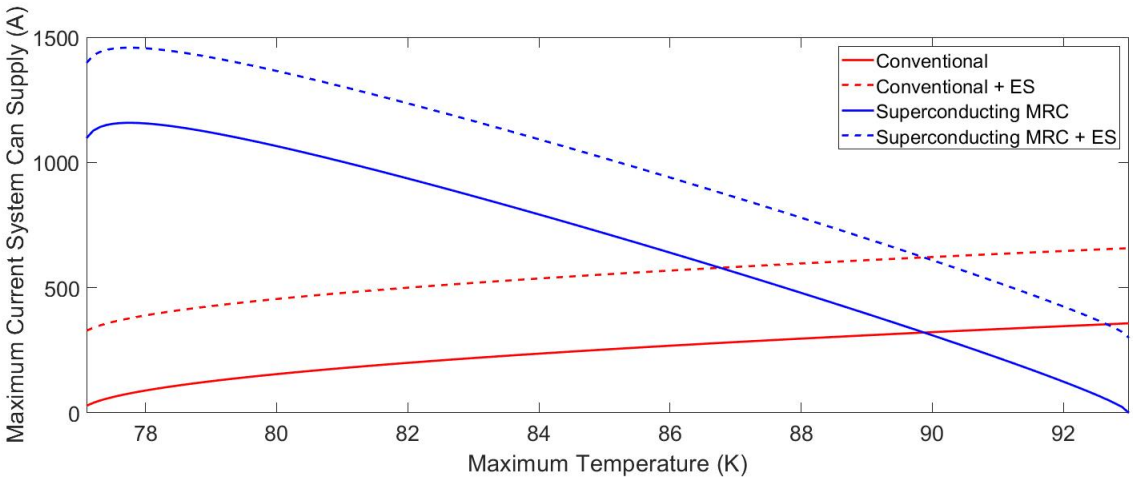

Fig. 12. Maximum current that can be supplied by the system using conventional current rating and superconducting MRC

fans as these will generate significant drag if de-energised [4]. In addition, the utilisation of V4C also has the benefit of preventing unnecessary over-curtailment, or removal from the circuit, of superconducting feeders, reducing the reliance on energy storage sources in the network during such conditions. This has the potential to reduce the extent of required redundancy and stored energy capacity implemented within the network architecture, potentially facilitating a reduction in system weight.

The results presented show that the effectiveness of V4C depends ultimately on the architecture of the network, and the impact on stability is a function both of where the current limitation is implemented within the system and the nature of the loads (constant power or constant impedance). In particular, the constant power nature of propulsion motor loads has been shown to cause the greatest destabilising effect, requiring local-to-load energy storage to maintain stability and full thrust provision whilst managing cable temperature. To further understand the system-level impacts of this control, future research will need to determine the operating constraints of superconducting propulsion motors. This could impact future superconducting TeDP network topologies that require reduced power operating modes by affecting the location of within the system, and technology choice of, the ESS. Results indicate that the ESS will require to be high-bandwidth, as well as requiring an interface with current limiting capable converter topologies (i.e MMC).

The full hardware validation of the V4C concept within a superconducting network remains a challenge in the short term. However, there is scope for a complementary follow-on activity to establish the level of accuracy attainable with the model-based temperature estimation algorithm, which would allow refinement of V4C through tuning of threshold safety margins. Future work identified by the authors is to identify the platform level benefits and challenges of this approach when the control is applied to multiple feeders within a single channel of the electrical power system.

ACKNOWLEDGMENT

This work was carried out as part of the Rolls-Royce University Technology Centre program at the University of Strathclyde.

REFERENCES

[1] Airbus, "Global Market Forecast 2018-2037: Global Networks, Global Citizens," 2018. [Online]. Available: https://www.airbus.com/aircraft/market/global-market-forecast.html

[2] E. Greitzer, P. Bonneyfoy, E. De la Rosa Blanco, and E. Al, "Volume 1 : N + 3 Aircraft Concept Designs and Trade Studies," NASA, Tech. Rep. March, 2010.

[3] M. Darecki, C. Edelstenne, T. Enders, E. Fernandez, P. Hartman, J. Herteman, M. Kerkloh, I. King, P. Ky, M. Mathieu, G. Orsi, G. Schotman, C. Smith, and J. Wörner, "Flightpath 2050," *Flightpath 2050 Europe's Vision for Aviation*, 2011. [Online]. Available: http://ec.europa.eu/transport/modes/air/doc/flightpath2050.pdf

[4] M. Kero, "Turboelectric Distributed Propulsion Test Bed Aircraft," Rolling Hills Research Coporation, El Segundo, Tech. Rep., 2013.

[5] C. Jones, P. Norman, S. Galloway, M. Armstrong, and A. Bollman, "Comparison of Candidate Architectures for Future Distributed Propulsion Aircraft," *IEEE Transactions on Applied Superconductivity*, vol. 26, no. 6, 2016.

[6] C. E. Jones, P. J. Norman, S. J. Galloway, M. J. Armstrong, and A. M. Bollman, "Future Distributed Propulsion Aircraft," *IEEE Transactions on Applied Superconductivity*, vol. 26, no. 6, 2016.

[7] D. C. Loder, A. Bollman, and M. J. Armstrong, "Turbo-electric Distributed Aircraft Propulsion: Microgrid Architecture and Evaluation for ECO-150," in *2018 IEEE Transportation and Electrification Conference and Expo, ITEC 2018*. Long Beach, CA, USA: IEEE, 2018, pp. 488–493.

[8] M. J. Armstrong, M. J. Blackwelder, A. M. Bollman, C. A. H. Ross, A. Campbell, C. E. Jones, and P. J. Norman, *Architecture, Voltage, and Components for a Turboelectric Distributed Propulsion Electric Grid*, 2015, no. July 2015. [Online]. Available: https://ntrs.nasa.gov/search.jsp?R=20150014237

[9] M. Armstrong, "Superconducting Turboelectric Distributed Aircraft Propulsion," Tuscon, USA, 2015. [Online]. Available: https://indico.cern.ch/event/344330/contribution/806654/attachments/677841/931299/Armstrong_CEC-ICMC_Conference_.pdf

[10] Steven M. Blair, "The Analysis and Application of Resistive Superconducting Fault Current Limiters in Present and Future Power Systems," Ph.D. dissertation, University of Strathclyde, 2013.

[11] J. Rivenc, G. Peres, F. Berg, L. Prisse, P. Rostek, D. Melyukov, V. Amelichev, and S. Samoilenkov, "An Evaluation of High Temperature Superconducting Power Cables for Airborne Application," in *2018 AIAA/IEEE Electric Aircraft Technologies Symposium (EATS)*. Cincinnati, Ohio: AIAA, 2018, pp. 1–21.

[12] L. Bottura, "Cable stability," Cern, Geneva, Switzerland, Tech. Rep., 2014. [Online]. Available: https://cds.cern.ch/record/1974064/files/arXiv:1412.5373.pdf

[13] K. Sivasubramaniam, T. Zhang, A. Caiafa, X. Huang, M. Xu, L. Li, E. T. Laskaris, and J. W. Bray, "Transient capability of superconducting devices on electric power systems," *IEEE Transactions on Applied Superconductivity*, vol. 18, no. 3, pp. 1692–1697, 2008.

[14] A. Ishiyama and H. Asai, "A stability Criterion for Cryocooler-Cooled HTS Coils," *IEEE Transactions on Appiled Superconductivity*, vol. 11, no. 1, pp. 1832–1835, 2001.

[15] C. E. Bruzek, A. Allais, K. Allweins, D. Dickson, N. Lallouet, and E. Marzahn, *Using superconducting DC cables to improve the efficiency of electricity transmission and distribution (T&D) networks: An overview*. Elsevier Ltd, 2015. [Online]. Available: http://dx.doi.org/10.1016/B978-1-78242-029-3.00006-6

[16] S. Nolan, C. Jones, P. Norman, and G. Burt, "Protection Requirements Capture for Superconducting Cables in TeDP Aircraft Using a Thermal-Electrical Cable Model," *SAE Technical Paper Series*, vol. 1, 2017.

[17] J. Hoelzen, Y. Liu, B. Bensmann, C. Winnefeld, A. Elham, J. Friedrichs, and R. Hanke-Rauschenbach, "Conceptual Design of Operation Strategies for Hybrid Electric Aircraft," *Energies*, vol. 11, no. 1, p. 217, 2018.

[18] S. Fletcher, "Protection of Physically Compact Multiterminal DC Power Systems," Ph.D. dissertation, University of Strathclyde, 2013.

[19] M. K. AL-Nussairi, R. Bayindir, S. Padmanaban, L. Mihet-Popa, and P. Siano, "Constant power loads (CPL) with Microgrids: Problem definition, stability analysis and compensation techniques," *Energies*, vol. 10, no. 10, 2017.

[20] F. Gao, S. Bozhko, A. Costabeber, G. Asher, and P. Wheeler, "Control Design and Voltage Stability Analysis of a Droop-Controlled Electrical Power System for More Electric Aircraft," *IEEE Transactions on Industrial Electronics*, vol. 64, no. 12, pp. 9271–9281, 2017.

[21] J. M. Guerrero, M. Chandorkar, T. L. Lee, and P. C. Loh, "Advanced control architectures for intelligent microgridspart i: Decentralized and hierarchical control," *IEEE Transactions on Industrial Electronics*, vol. 60, no. 4, pp. 1254–1262, 2013.

[22] F. Gao, S. Bozhko, S. Yeoh, G. Asher, and P. Wheeler, "Stability of multi-source droop-controlled Electrical Power System for more-electric aircraft," *2014 IEEE International Conference on Intelligent Energy and Power Systems, IEPS 2014 - Conference Proceedings*, pp. 122–126, 2014.

[23] X. Giraud, H. Piquet, M. Budinger, X. Roboam, M. Sartor, and S. Vial, "Knowledge-based system for aircraft electrical power system reconfiguration," *Electrical Systems for Aircraft, Railway and Ship Propulsion, ESARS*, vol. 2048, pp. 1–6, 2012.

[24] D. Schlabe and J. Lienig, "Energy management of aircraft electrical systems - State of the art and further directions," *Electrical Systems for Aircraft, Railway and Ship Propulsion, ESARS*, pp. 1–6, 2012.

[25] O. Meier, D. Scholz, and I. D. Scholz, "A Handbook Method for the Estimation of Power Requirements for Electrical De-Icing Systems," in *Deutscher Luft- und Raumfahrt Kongress*, 2010. [Online]. Available: https://www.fzt.haw-hamburg.de/pers/Scholz/MOZART/MOZART_PUB_DLRK_10-08-31.pdf

[26] S. Wang, J. Tang, and F. Younce, "Temperature Measurement," pp. 987–993, 2007. [Online]. Available: www.electronics-cooling.com/2007/08/thermal-diffusivity/S

[27] W. T. B. de Sousa, "TRANSIENT SIMULATIONS OF SUPERCONDUCTING FAULT CURRENT LIMITERS," Ph.D. dissertation, Federal University of Rio de Janeiro, 2015.

[28] S. Stavrev, "Modelling of High Temperature Supraconductors for AC Power Applications," Ph.D. dissertation, Swiss Federal Institute of Technology Lausanne, 2002.

[29] D. Colangelo and B. Dutoit, "Impact of the normal zone propagation velocity of high-temperature superconducting coated conductors on resistive fault current limiters," *IEEE Transactions on Applied Superconductivity*, vol. 25, no. 2, pp. 1–7, 2015.

[30] R. Ottersten, "On Control of Back-to-Back Converters and Sensorless Induction Machine Drives Department of Electric Power Engineering," Ph.D. dissertation, Chalmers University of Technology, 2003.

[31] R. D. Donkcer, D. Pulle, and A. Veltman, *Advanced Electrical Drives Analysis, Modeling, Control*. Springer, Dordrecht, 2011.

[32] V. Blasko and V. Kaura, "A new mathematical model and control of a three-phase AC-DC voltage source converter," *Power Electronics, IEEE Transactions on*, vol. 12, no. 1, pp. 116–123, 1997.

[33] J. M. Guerrero, J. C. Vasquez, J. Matas, L. G. De Vicuña, and M. Castilla, "Hierarchical control of droop-controlled AC and DC microgrids - A general approach toward standardization," *IEEE Transactions on Industrial Electronics*, vol. 58, no. 1, pp. 158–172, 2011.